Title
Context-Specific Function of S6K2 in Th Cell Differentiation

Journal
The Journal of Immunology, 197(8)

ISSN
0022-1767

Authors
Pai, Christine
Walsh, Craig M
Fruman, David A

Publication Date
2016-10-15

DOI
10.4049/jimmunol.1600167

Peer reviewed

Context-specific function of S6K2 in helper T cell differentiation[1]

Christine Pai[*], Craig M. Walsh[*], David A. Fruman[*†]

Running title: S6K2 function in helper T cell differentiation

[*] Department of Molecular Biology & Biochemistry, and Institute for Immunology, University of California, Irvine. Irvine, CA 92697.

[†]Address correspondence to: David A. Fruman, 3242 McGaugh Hall, University of California, Irvine. Irvine, CA 92697-3900. Email: dfruman@uci.edu

[1] This work was supported by NIH grant R21-AI099656 (to D.A.F.) and National Multiple Sclerosis Society CA1058-A8 (to C.M.W.).

Abstract

The mammalian target of rapamycin (mTOR) is essential for helper T cell proliferation and effector differentiation, making the mTOR signaling network an attractive immunomodulatory target for autoimmune related diseases. While direct targeting of mTOR-complex-1 (mTORC1) with rapamycin can provide clinical benefit, targeting downstream enzymes has potential to offer more selective immunosuppression. Here we evaluated p70 ribosomal protein S6 Kinase 2 (S6K2), a downstream effector of mTORC1, for its role in T cell function and autoimmunity. S6K2 is a direct substrate of mTORC1, with a potential role in Th17 differentiation suggested by biochemical studies. Using a genetic approach with S6K2 knockout mice, we found that S6K2 loss reduces Th17 skewing and increases Treg differentiation *in vitro* when cultured in RPMI media. However, S6K2 was dispensable for Th17 differentiation in IMDM media. In an *in vivo* EAE model in which rapamycin suppresses disease, S6K2 knockout mice did not exhibit differences in clinical score or Th17 differentiation. These results suggest that S6K2 is dispensable for Th17-driven autoimmunity and highlight how distinct experimental conditions can produce significantly different results in T cell differentiation.

Introduction

The mTOR protein is a serine-threonine kinase that forms two separate complexes, mTORC1 and mTORC2. Each complex has distinct regulation and downstream target substrates (1, 2). mTOR signaling in both naïve $CD4^+$ and $CD8^+$ T cells can be activated by engagement of a recognized antigen through the PI3K-Akt-mTOR pathway (3, 4). The complex mTORC1, defined by the regulatory-associated protein of mTOR (Raptor) subunit, regulates both bioenergetic and biosynthetic processes that are crucial for T cell growth and division (5, 6). These include protein translation, lipid biogenesis, and suppression of autophagy. Downstream of mTORC1, two directly phosphorylated substrates are ribosomal S6 Kinases (S6Ks) and eukaryotic initiation factor 4E (eIF4E) binding proteins (4E-BPs), both of which have evolutionarily conserved roles in cell growth and metabolism (1, 7, 8).

Newly activated T-lymphocytes utilize mTOR signaling to initiate transcription of metabolic regulatory genes (9), a process crucial for driving proliferation and differentiation. The ability to produce a sustainable effector program selectively requires mTORC1 activity to integrate both immune and nutrient cues. In the context of an autoimmune response, proinflammatory Th1 and Th17 subsets are highly dependent upon glucose consumption, whereas suppressive Tregs favor increased mitochondrial respiration (10–12). Interestingly, while mTORC1 activity is required for differentiation and effector cytokine production of both Th1 and Th17 subsets (13, 14), the production of induced Tregs increases when mTORC1 is suppressed (13, 15, 16). The function of established Tregs is impaired when mTORC1 activity is either reduced (12) or increased (17).

Rapamycin, a potent inhibitor of mTORC1 activity, suppresses pathology in several animal models of T cell-driven autoimmunity (18–22) and at low doses extends lifespan of mice (23). Rapamycin has been tested in clinical trials of human autoimmune diseases and is often prescribed to such patients off label (24–26). However, sustained rapamycin treatment has some detrimental side effects (27, 28). Targeting mTORC1 substrate pathways is a reasonable alternative that might provide a better therapeutic window.

There are two S6K isoforms, S6K1 and S6K2, both of which are expressed in T cells (29, 30). Activated mTORC1 phosphorylates S6Ks, which in turn phosphorylate the ribosomal protein S6 and other substrates involved in protein and lipid biosynthesis (7). When mTORC1 phosphorylates 4E-BPs, these proteins are released from eIF4E to promote cap-dependent translation (31). Thus, S6K and 4E-BP signaling pathways converge to regulate mRNA translation. The inhibition of mTORC1 by rapamycin results in profound suppression of S6K phosphorylation and activity (32, 33), but only partial inhibition of 4E-BP1 phosphorylation (34). However, it is unclear which mTOR functions are mediated by S6Ks during T helper (Th) cell differentiation.

Previous studies have provided limited and sometimes conflicting information about the functions of S6Ks in T cell growth, proliferation and differentiation. *S6K1*$^{-/-}$ mice have a small size phenotype but apparently normal lymphocyte function, associated with massive compensatory upregulation of S6K2 in T cells (30). One study reported that the S6K1 inhibitor PF-4708671 suppresses CD4 T cell growth and proliferation (35). However, we found that PF-4708671 has non-specific effects at the 10μM concentration used (36). Mice with a germline deletion of both *S6K1* and *S6K2* exhibit perinatal lethality, making it challenging to analyze mature immune cells (37). In the few adult

double knockout mice that survive, T cell growth and proliferation is surprisingly unimpaired (36). Koyasu and colleagues used gain-of-function approaches to suggest unique roles for S6K1 and S6K2 in Th17 differentiation (14). A later study by Sasaki *et al.* (38) utilized *S6K1*$^{-/-}$ mice to show a role for S6K1 in differentiation of Th17 cells, but not other CD4^{+} T cell subsets. S6K1 was found to promote expression of Th17 associated genes (e.g. *IL17a*, *IL17f*, and *IL23R*); however, it did not affect expression of the Th17 master transcription factor retinoic acid receptor-related orphan receptor gamma (RORγ). In addition, mice lacking S6K1 did not show improvement of clinical disease scores in experimental autoimmune encephalomyelitis (EAE), a mouse autoimmunity model.

In this study, we investigated the specific role(s) of S6K2 in mouse T cell activation, development, and proliferation. S6K2 germline knockout mice are viable, fertile and of normal size; moreover, S6K1 expression is unchanged in S6K2-deficient T cells. We found that S6K2 knockout (*S6K2*$^{-/-}$) mice had no defects in T cell development and early CD4 T cell activation, despite a measurable decrease in overall S6K activity as determined by S6 protein phosphorylation. Interestingly, *S6K2*$^{-/-}$ cells exhibited a context-specific Th differentiation phenotype. *In vitro* experiments using RPMI culture media revealed decreased Th17 and increased Treg differentiation in *S6K2*$^{-/-}$ cells. However, in an *in vivo* EAE model of autoimmunity, *S6K2*$^{-/-}$ mice showed no difference in clinical outcome or Th17 differentiation. Re-evaluation of the *in vitro* differentiation assay conditions surprisingly showed that the Th17 differentiation defect depends on the culture medium used. IMDM medium, known to induce more robust Th17 differentiation (39), led to Th17 skewing and robust proliferation that was indistinguishable between *S6K2*$^{-/-}$ and wildtype T cells. This unexpected result indicates that S6K2 is dispensable

for Th17 differentiation under optimal activation conditions. In addition, our findings suggest that the use of IMDM media for *in vitro* Th17 studies better predicts the *in vivo* response in EAE models.

Materials and Methods

Animals

All mice were kept in specific pathogen–free animal facilities and in accordance with guidelines of the University of California Institutional Animal Care and Use Committee. C57BL/6 mice were obtained from Jackson Laboratories. *S6K2*$^{-/-}$ mice were a gift from Sara Kozma.

Media and cell culture

Primary cell culture was performed in complete media consisting of RPMI or IMDM media (Gibco) supplemented with 10% FCS (Gibco), L-glutamine (Corning), ßME and antibiotics (Gibco).

Antibodies and reagents

Stimulatory anti-CD3 (2C11) and anti-CD28 (37.51), as well as neutralizing anti-IFN-γ (XMG1.2), anti-IL-2 (JES6-1A12), anti-IL-12p40 (C17.8), and anti-IL-4 (11B11) were from eBioscience. For differentiation, recombinant cytokines were used: TGF-beta (R&D systems), mouse IL-6 and IL-12 (eBioscience). For flow cytometry analysis, surface and intracellular staining antibodies were purchased from eBioscience and Cell Signaling Technologies. For immunoblotting, rabbit antibodies specific for total and phosphorylated forms were obtained from Cell Signaling Technologies: AKT (#2965, #9267, #4058, #4685), rS6 (#4838, #2215, #2211), S6K (#9205, #2708), pCAD (#12662). For imaging, anti-Mouse RORγt (B2D) from eBioscience was used.

Cell purification

Splenic $CD4^+$ T cells depleted of natural Tregs were purified by negative selection using the EasySep Mouse $CD4^+$ T Cell Isolation Kit from Stemcell Technologies with biotinylated anti-CD25 (0.5 µg/ml) added.

Cell cycle analysis

T cells were stimulated in T-conventional (Tconv), Th17, or Treg skewing conditions for 40h and fixed with 100% ethanol. Cells were incubated with RNAse A and propidium iodine (PI) diluted in cell cycle buffer (5mM EDTA in PBS) before cell cycle analysis was performed using FACS.

Cell stimulation and differentiation

Unless otherwise stated, T cells were stimulated as Tconv, with plate-bound anti-CD3 (5 µg/ml) and soluble anti-CD28 (2 µg/ml) from eBioscience. 10 nM of Rapamycin (LC Laboratories) and 500 nM of LY2584702 (S6K1i) (Eli Lilly & Company) were also used when indicated. When proliferation is measured, isolated T cells were prelabeled with CFSE (eBioscience). Cell stimulation cocktail (500x) from eBioscience containing PMA (phorbol 12-myristate 13-acetate), ionomycin, Brefeldin A, and monensin were used for restimulation (detection of intracellular cytokines). For Th polarization assays, isolated naïve T cells were skewed with anti-CD3 and anti-CD28 for 4 days (unless otherwise noted), restimulated for 4 hours, and harvested for flow cytometry analysis. Skewing conditions were as follows: T_H1- IL-12 (20 ng/ml) and anti-IL-4 (10 µg/ml); T_H17, TGF-

β (5 ng/ml), IL-6 (20 ng/ml), anti-IFN-γ (10 μg/ml), anti-IL-4 (10 μg/ml) and IL-2 (1 ng/ml); T_{reg}, TGF-β (5 ng/ml).

Intracellular staining for flow cytometry analysis

After restimulation with cell stimulation cocktail, cells were fixed and made permeable with BD Cytofix/Cytoperm and then stained for cell surface markers and cytokines. Intracellular staining of transcription factors (i.e. FoxP3) was done without restimulation. Gates were set appropriately with unstimulated controls and voltages were set on the basis of isotype-matched control antibodies. Data were acquired using a BD FACSCalibur flow cytometer (BD Biosciences) and analyzed using FlowJo software (Tree Star).

ELISA

Cells were harvested after indicated stimulation periods and supernatants were collected to measure cytokine production according to manufacturer's instructions. IL-2 and IL-10 ELISA kits were obtained from eBioscience and IL-17A ELISA kit was obtained from R&D systems.

Experimental Autoimmune Encephalomyelitis

10-12 week-old female wildtype and $S6K2^{-/-}$ mice were immunized with 100μg of MOG_{35-55} antigen in 200μg of CFA per mouse. Pertussis was administered i.v. on day 0 and 1 at 400ng per injection. Mice were scored on a scale of 0–5: 0-no clinical symptoms; 1-limp tail; 2- limp tail and partial hind limb paralysis; 3- limp tail and

complete hind limb paralysis; 3.5- partial front or one-sided paralysis; 4- moribund; 5- death. Mice scoring 3.5 or more for two consecutive days were euthanized. Spinal cords were harvested and centrifuged through a Percoll gradient. Isolated infiltrating lymphocytes were restimulated for 4h before staining intracellularly for IFNγ and IL-17A. To analyze the phenotype of activated $CD4^+$ T cells during disease induction, wildtype and $S6K2^{-/-}$ mice were immunized with MOG peptide without pertussis and sacrificed after 10 days. Lymph nodes were harvested for analysis of the percentage of $pS6^+$ among $CD4^+CD44^{hi}$ cells. Splenocytes were restimulated with MOG (10 and 50µg/mL), IL-23 (20ng/mL), and anti-IFNγ antibody (10µg/mL) for 3 days and then harvested for cytokine measurement in the supernatant, as well as stained intracellularly for IL-17A and FoxP3 expressing $CD4^+$ T cells.

Immunofluorescence Microscopy

$CD4^+$ T cells were harvested after 40 hours of stimulation, washed, and centrifuged. The pellets were fixed with 4% formaldehyde for 10 min at 37°C, permeabilized with 0.1% Saponin (Acros Organics) in PBS for 10 min at room temperature, blocked with 5% anti-rat serum in 1X PBS / 0.1% Saponin and stained with anti-mouse RORγT (eBioscience) for 2 hr at 37°C in PBS containing 1% BSA / 0.1% Saponin. F(ab')2 Anti-Rat IgG PE (eBioscience) were used as a secondary antibody. Specimens were further stained with DAPI (Thermo Fisher Scientific) and Rhodamine-phalloidin (Thermo Fisher Scientific). Single cell suspensions are spun onto a microscope slide by use of a cytocentrifuge Images were obtained using a Leica TCS SP8 confocal scanning microscope and LAS X core microscopy software. For statistical analysis, the Manders'

Overlap Coefficient was used to measure RORγ localization in the nucleus (as determined by RORγ and DAPI staining overlap) in at least three representative fields of view for each condition.

Metabolic studies

Metabolic flux analysis was performed in complete Seahorse media (Seahorse Bioscience, 102365) supplemented with 25mM D-Glucose, 1mM Na-Pyruvate and 2mM L-glutamine.

Treg suppression assays

nTregs were sorted by $CD4^+CD25^+$ expression from combined spleen and lymph nodes of aged matched mice. nTregs were then seeded with CFSE labeled naïve WT $CD4^+$ T cells at a 1:2 ratio. The wells were pre-coated with 2µg/mL of CD3 and 1µg/mL of soluble CD28 was added. After 3 days of stimulation, the cells were washed and analyzed by FACS.

Statistical Analysis

Mean and SEM values were calculated from at least three independent experiments. *p* values were calculated using a two-tailed unpaired Student's t-test when determining differences between groups, unless the Wilcoxon signed-rank test was used to determine pairwise differences (specifically indicated in figure legends).

Results

S6K2$^{-/-}$ mice have normal T cell development and proliferation

S6K2$^{-/-}$ mice are viable, fertile, and exhibit normal development. They exhibit no evidence of autoimmunity or inflammatory conditions. Using these mice, we sought to determine the role of S6K2 in T cell development and activation. Analysis of peripheral lymphoid organs in *S6K2*$^{-/-}$ mice revealed normal percentages and ratios of CD4^{+} and CD8^{+} populations (Fig. 1A and 1B), and developing T cell subpopulations in the thymus were indistinguishable (Fig. 1A and 1B). Natural Treg (nTreg) populations (CD4^{+}CD25^{+}) were also comparable in percentage in the peripheral lymphoid organs (Fig. 1C). The suppressive ability of nTregs was comparable when comparing CD4^{+}CD25^{+} cells sorted from WT versus S6K2$^{-/-}$ mice (Supplemental Fig. 1A).

We then isolated naïve conventional T cells (CD4^{+}CD25^{-}) and stimulated them with anti-CD3 and anti-CD28 for 24h to assess the role of S6K2 in early T cell activation. Expression of the activation markers CD25 and CD69, and the induction of blasting as measured by forward scatter, were similar between wildtype (WT) and *S6K2*$^{-/-}$ T cells (Fig. 1D). Production of IL-2 after 40hr stimulation was also unimpaired (Supplemental Fig. 1B).

Upon TCR engagement, the enzymes PI3K and Akt are essential for the induction of numerous signaling cascades (4). mTORC1 is a main effector downstream of PI3K and Akt, yet little is known about the roles of S6Ks in these processes. First we assessed the contribution of S6K2 to total S6K activity. Naïve T cells were stimulated for different times and analyzed by flow cytometry to measure phosphorylation of the S6 ribosomal protein (pS6). Phosphorylation of S6 at the Ser 240 and 244 residues (pS6) is S6K-

dependent and a robust readout of mTORC1 and S6K activity (37, 40). This analysis revealed that *S6K2*$^{-/-}$ T cells have a reduction in the fraction of cells with high pS6 at early time points, and a delayed increase in pS6 positive cells when compared to WT T cells (Fig. 2A). Focusing on the 24hr time point, we observed a significant reduction in both the MFI and fraction of the population positive for pS6 in *S6K2*$^{-/-}$ cells (Fig. 2B). Rapamycin was used as a positive control to show that the pS6 measurements were completely mTORC1-dependent. We also assessed the contribution of S6K1 to this response using the selective inhibitor LY2584702 (here termed S6K1i) (41). We used S6K1i instead of *S6K1*$^{-/-}$ mice because of the reported compensatory upregulation of S6K2 in such mice (30). The results showed that S6K1 inhibition strongly suppressed the activation-induced increase in pS6 in both WT and *S6K2*$^{-/-}$ T cells.

We recently demonstrated that S6Ks are surprisingly dispensable for both growth and division in activated T cells (36). Confirming these findings, *S6K2*$^{-/-}$ T cells showed comparable proliferation to WT T cells at 72hr (Fig. 2C and D). At an earlier time point of 40hr, there was no difference in cell cycle distribution between WT and *S6K2*$^{-/-}$ T cells (Supplemental Fig. 1C). Addition of S6K1i to both *S6K2*$^{-/-}$ and WT T cells also did not impair their proliferation despite fully suppressing pS6 induction (Fig. 2C). Similarly, there was no difference in growth (cell size measured by forward scatter (FSC)) in WT and *S6K2*$^{-/-}$ T cells treated with or without the S6K1i inhibitor (Fig. 2E and 2F). We also tested allogeneic stimulation by mixed lymphocyte reaction and also observed no difference in proliferation or cell death (data not shown). These results show that in the absence of S6K activity, T cells are still able to grow and proliferate under neutral stimulation conditions.

Distinct signaling roles for S6K1 and S6K2

The first study of *S6K1*$^{-/-}$ mice reported that S6K1-deficient lymphocytes have a compensatory upregulation of S6K2, even under resting conditions (30). To determine whether *S6K2*$^{-/-}$ T cells have altered expression of S6K1, we used Western blots to measure total S6K1 in resting and 24h stimulated T cells. S6K1 expression in the *S6K2*$^{-/-}$ was similar to WT T cells under basal and activated conditions (Fig. 3A and 3B). This confirms that S6K1 is not upregulated to compensate for loss of S6K2 in the *S6K2*$^{-/-}$ T cells.

In many cells, S6K1 mediates strong negative feedback on growth factor receptor signaling and the activation of PI3K and AKT (42). Consequently, inhibition of mTORC1 or S6K1 often leads to increased phosphorylation of Akt (pAkt). In accord, WT naïve T cells treated with S6K1i had a statistically significant increase in pAkt following TCR stimulation (Fig. 3C). This increase was not observed in *S6K2*$^{-/-}$ T cells, which instead showed a variable reduction in pAkt. These results are in accord with a study of breast cancer cells, which reported reduced pAkt when S6K2 was suppressed (43). We also measured phosphorylated CAD, reported to be a selective substrate of S6K1 (44, 45). CAD is essential for the *de novo* synthesis of pyrimidine nucleotides and is directly phosphorylated by S6K1 at Ser1859. Though S6K1i significantly reduced pCAD in activated WT T cells, loss of S6K2 had no apparent effect (Fig. 3A and 3B). These signaling studies support the conclusion that S6K1 and S6K2 have distinct substrates in activated T cells and contribute differently to feedback pathways.

S6K2$^{-/-}$ mice generate more Tregs and fewer Th17s *in vitro*

Although *S6K2*$^{-/-}$ T cells proliferated normally under neutral stimulation conditions, we considered the possibility that S6K2 deficiency impairs proliferation and differentiation under T helper skewing conditions. For these *in vitro* differentiation assays, highly purified naïve CD4^{+}CD25^{-} T cells were labeled with CFSE and activated with under conditions that polarize cells towards Th1, Th17, or Treg differentiation. On day 4, the cells were harvested and stained for intracellular cytokines or transcription factors indicative of each subset. Though S6K2 loss did not affect skewing to the Th1 subset, the percentage of IL-17-producing cells was reduced under Th17 culture conditions when compared to WT T cells (Fig. 4A and 4B). Conversely, *S6K2*$^{-/-}$ T cells showed an increased percentage of FoxP3+ cells when stimulated under Treg skewing conditions (Fig. 4 and 4B). Importantly, *S6K2*$^{-/-}$ T cells showed unimpaired IL-2 production (Supplemental Fig. 1B) and cell cycle distribution at 40hr (Supplemental Fig. 1D), and proliferation was comparable to WT T cells at 72hr for both Th17 and Treg subsets (Fig. 4C), indicating that altered differentiation was not linked to changes in cell division.

Next we measured IL-10 production under Treg skewing conditions and IL-17A production under Th17 conditions, 4 days after stimulation. WT and *S6K2*$^{-/-}$ T cells produced comparable amounts of each cytokine, though there was a trend towards increased IL-10 production by *S6K2*$^{-/-}$ T cells (Fig. 4D).

S6K2 deficiency does not ameliorate EAE clinical symptoms

Drawing upon our findings of reduced Th17 and increased Treg generation *in vitro*, we tested whether *S6K2*$^{-/-}$ mice were protected from autoimmune disease in a mouse model. We chose MOG_{35-55} induced experimental autoimmune encephalomyelitis (EAE), a classical mouse model of multiple sclerosis (MS) in which Th17 cells are required and mTORC1 activity plays a prominent role (13, 14, 46, 47). The pathogenesis of EAE is strongly reinforced by a Th17/Treg imbalance (48). Surprisingly, disease onset and severity was comparable in *S6K2*$^{-/-}$ and WT mice (Fig. 5A). We also quantitated cytokine production of infiltrating lymphocytes in the spinal cord and found similar percentages of IFNγ and IL-17A producing $CD4^+$ T cells (Supplemental Fig. 1E). To confirm the role of mTORC1 in our hands, we conducted a second EAE experiment comparing WT mice treated with rapamycin or vehicle. As reported (13, 19), rapamycin treatment significantly lowered EAE scores (Fig. 5B) and reduced the percentage of CD4 T cells producing IFNγ or IL-17A in the spinal cord (Fig. 5C). Concurrently, we analyzed cohorts of WT and *S6K2*$^{-/-}$ mice that were not injected with rapamycin or vehicle. Again the absence of S6K2 did not affect EAE onset or severity (Fig. 5B), and did not affect inflammatory cytokine production in $CD4^+$ T cells isolated from spinal cord infiltrates (Fig. 5C).

Because we did not detect any differences in proinflammatory responses at the peak of disease, MOG immunization was also used to characterize T effector and Treg responses *in vivo* during immune response development. Cohorts of WT and *S6K2*$^{-/-}$ mice were immunized with MOG_{35-55} without pertussis to characterize T cell differentiation. This model allows assessment of antigen-specific immune responses to complement polyclonal *in vitro* differentiation assays. After 10 days, the mice were sacrificed and

lymph nodes were harvested to measure pS6 amounts in $CD4^+CD44^{hi}$ T cells. WT and *S6K2*$^{-/-}$ cells had similar pS6 as measured by both MFI and % positive (Fig. 5D). Splenocytes were restimulated with MOG peptide in cultures that included IL-23 and anti-IFNγ antibody for 3 days, to specifically measure frequencies of MOG-specific Th17 and Treg cells. Though the percentage and MFI of $CD4^+IL17A^+$ T cells were no different, $CD4^+FoxP3^+$ populations was significantly increased in cultures from *S6K2*$^{-/-}$ mice (Fig. 5E). IL-17 production measurement by ELISA also showed no difference between WT and *S6K2*$^{-/-}$ mice (Supplemental Fig. 1F). In summary, our data suggest that S6K2 is not required for *in vivo* Th17 differentiation, but does seems to suppress Treg generation in this model.

The role of S6K2 in Th17 differentiation is context-specific

To understand why significant *in vitro* differences between *S6K2*$^{-/-}$ and WT T cells did not translate into altered Th17 differentiation *in vivo*, we reassessed the cell culture media used for T cell differentiation. We initially used RPMI media, which is commonly used for primary lymphocyte culture but supports very low levels of Th17 differentiation (39). Thus, we compared RPMI to IMDM, the latter a medium rich in aromatic amino acids that was shown to support robust Th17 differentiation (39). Not only did IMDM media enhance Th17 skewing in WT T cells, it also restored Th17 differentiation of *S6K2*$^{-/-}$ cells to levels equivalent to WT (Fig. 6A and Supplemental Fig. 2A). In contrast to the rescue of Th17 differentiation, *S6K2*$^{-/-}$ T cells in IMDM still generated a higher percentage of FoxP3+ cells under Treg skewing conditions compared to WT (Fig. 6A).

IL-17A and IL-10 cytokine production under Th17 and Treg skewing conditions, respectively, were comparable between WT and *S6K2*$^{-/-}$ T cells (Fig. 6C).

The tryptophan metabolite 6-formylindolo[3,2-b] carbazole (FICZ) found in IMDM can enhance differentiation of Th17 cells in RPMI media (39). Therefore, we supplemented RPMI with 300 nm FICZ to see if this could account for restored Th17 differentiation in *S6K2*$^{-/-}$ T cells. Indeed, the proportion of IL-17^{+} cells was comparable between WT and *S6K2*$^{-/-}$ T cells when cultured in RPMI plus FICZ (Fig. 6C and Supplemental Fig. 2B). Proliferation, however, was not restored to the robust response obtained using IMDM (Supplemental Fig. 2C). To further explore these media-based phenotypic differences, we measured mTORC1 signaling output as assessed by pS6 intracellular staining. 24hr after T cell stimulation under neutral conditions, cells cultured in IMDM exhibited significantly higher mTORC1 activity compared to cells cultured in RPMI, as assessed by the MFI of pS6 as well as the proportion of pS6-high cells (Fig. 6B). This difference was observed in both *S6K2*$^{-/-}$ and WT populations.

A previous study by Kurebayashi et al. reported that S6K2 functions downstream of mTORC1 to shuttle the Th17 transcription factor RORγ to the nucleus (14). This study did not assess the role of RORγ localization in Th17 differentiation in *S6K2*$^{-/-}$ T cells. Therefore, we measured nuclear localization of RORγ in WT and *S6K2*$^{-/-}$ T cells after 40hr of stimulation in Th17 conditions, comparing both RPMI and IMDM media. In RPMI, *S6K2*$^{-/-}$ T cells indeed showed significantly reduced RORγ nuclear localization when compared to WT T cells (Supplemental Fig. 3A). Culturing cells in IMDM media resulted in significantly increased nuclear localization for *S6K2*$^{-/-}$ T cells, but did not

rescue this to WT levels (Supplemental Fig. 3B). WT cells cultured in IMDM did not exhibit an increase in RORγ nuclear localization compared to RPMI conditions.

Because mTORC1 activity is strongly tied to cell metabolism, we used a Seahorse metabolic flux analyzer to analyze metabolism in both WT and S6K2$^{-/-}$ cells activated in Th17, Treg, and neutral (Tneu) differentiation conditions. In these experiments, initial stimulation was done in IMDM media for Th17 conditions and RPMI for Tneu and Treg conditions. Interestingly, basal glycolysis (extracellular acidification rate (ECAR)) and oxidative phosphorylation (oxygen consumption rate (OCR)) of all three subsets were not significantly different (Supplemental Fig. 4A and 4B). Rapamycin treated WT cells were used as a positive control in reducing both ECAR and OCR of Tneu stimulated cells (49).

Discussion

S6K1 and S6K2 are canonical mTORC1 substrates whose inhibition has potential to modulate T helper differentiation and treat T-cell mediated autoimmune diseases. Indeed, S6K1 knockdown reduces Th17 differentiation in both WT cells and in cells with hyperactive mTORC1 resulting from TSC1 deficiency (17). Although S6K2 is also prominently expressed in lymphocytes (29), the role of this isoform in T cells has not been investigated. Here we used S6K2$^{-/-}$ mice to assess the impact of S6K2 deficiency on T cell development, proliferation and differentiation. Previous genetic studies of T cells lacking mTOR pathway components (i.e. mTOR, raptor, and Rheb) have generally reported no changes in early T cell development and homeostasis. Our data show similarly that S6K2$^{-/-}$ T cells develop normally and that CD4^{+} T cells have no defects in early activation. This allowed us to ensure that functional studies were unaffected by

417 preexisting cell-intrinsic defects. Proliferation of S6K2$^{-/-}$ T cells was unimpaired under
418 neutral stimulation conditions or when polarized to Th1, Th17 or Treg subsets. Analysis
419 of T helper differentiation *in vitro* showed a modest but significant decrease in Th17
420 differentiation using RPMI media, but not in IMDM. Using MOG_{35-55}-induced EAE as an
421 *in vivo* model of Th17-driven autoimmunity, we compared WT and S6K2$^{-/-}$ mice and
422 observed comparable clinical scores and Th17 cell percentages in the spinal cord.
423 Utilizing the same model to study Th17 and Treg responses to a specific antigen *in vivo*,
424 we gated on CD4^{+}CD44^{hi} infiltrating T cells in the cervical lymph nodes and found no
425 change in pS6 signaling, which corresponds with the *in vitro* signaling data in cells
426 cultured in IMDM. We also restimulated splenocytes with MOG and detected no
427 difference between WT and S6K2$^{-/-}$ mice in IL-17A expression. However, there was a
428 significant increase in CD4^{+}FoxP3^{+} populations. These findings suggest that S6K2 may
429 play a negative role in Treg generation, but is not a key driver of Th17 differentiation or
430 autoimmune pathology *in vivo*, at least in this EAE model. Moreover, the discordant
431 findings using RPMI media compared to IMDM and to the EAE model emphasize the
432 importance of using optimal *in vitro* activation conditions for assessing Th17
433 differentiation.

434 Signaling measurements indicate a lesser role for S6K2 compared to S6K1 in
435 phosphorylation events triggered by TCR/CD3 engagement. The phosphorylation of S6
436 protein was modestly reduced within 24hr of activation, indicating that S6K2 contributes
437 significantly to the overall S6K signaling output. However, S6K1 blockade with the
438 selective inhibitor LY2584702 caused a stronger inhibition of pS6 at all time points
439 assessed. Furthermore, S6K1 inhibition but not S6K2 loss reduced phosphorylation of

CAD, a key enzyme in *de novo* pyrimidine synthesis (44, 45). mTORC1 and S6K1 mediate negative feedback loops that suppress upstream phosphorylation of Akt in many cellular systems (42, 50, 51). In accord, S6K1i treatment of WT T cells significantly increased pAkt, indicating a removal of feedback signaling. In contrast, pAkt in activated S6K2$^{-/-}$ T cells was similar or slightly reduced compared to WT cells. We also found that S6K1 is not upregulated in the absence of S6K2, whereas a study of S6K1$^{-/-}$ mice reported massive compensatory upregulation of S6K2 in T cells (30). These distinctions further support the conclusion that S6K1 loss has greater impact on T cell biology compared to S6K2 loss. Nevertheless, the fact that S6K2 is expressed in T cells suggests that this kinase has a functional role, prompting us to assess T cell proliferation and differentiation.

S6K2$^{-/-}$ T cells became activated (based on expression of CD25 and CD69 surface markers and production of IL-2) and proliferated (assessed by CFSE dilution at 72hr and cell cycle at 40hr) to a comparable extent as WT cells. In fact, when we fully suppressed S6K function by treating S6K2$^{-/-}$ T cells with S6K1i, proliferation was unimpaired. These data agree with our recent finding that S6Ks are dispensable for lymphocyte proliferation downstream of mTORC1; instead, the 4E-BP/eIF4E axis is the main driver of lymphocyte clonal expansion (36). It is reasonable to propose that the primary role of S6Ks in T cells is to control differentiation rather than proliferation. A role for S6K1 in Th17 differentiation is supported by both gain- and loss-of-function studies (14, 17). S6K2 can promote nuclear localization of RORγT, the Th17 cell hallmark transcription factor (14), but whether this function is required for Th17 differentiation has not been

462 determined. Therefore, we tested S6K2$^{-/-}$ CD4 T cells for the ability to differentiate into
463 Th17 and other Th cell subsets.

464 Our results show that S6K2 has a context-specific role in Th17 differentiation *in*
465 *vitro*. When CD4 T cells were cultured in RPMI media under Th17 polarizing conditions,
466 S6K2$^{-/-}$ cells generated a significantly lower percentage of IL-17A^{+} cells. This correlated
467 with reduced nuclear localization of RORγT. This finding is consistent with the model
468 that S6K2 and not S6K1 shuttles RORγT to the nucleus as proposed by Kurebayashi *et*
469 *al*. (14). Importantly, when cells were cultured in IMDM to support more robust Th17
470 differentiation (39), both WT and S6K2$^{-/-}$ CD4 T cells generated higher percentages of
471 IL-17A^{+} cells and there was no difference between the genotypes. The IMDM condition
472 also fully rescued the S6 phosphorylation defect in S6K2$^{-/-}$ T cells, and partially restored
473 nuclear localization of RORγT. It is not clear how the distinct composition of RPMI and
474 IMDM media can affect the wiring of signaling pathways, such as the S6K2-dependence
475 of S6 phosphorylation and RORγT localization. Compared to RPMI, IMDM has
476 increased D-glucose and L-glutamine amounts in addition to higher concentrations of
477 inorganic salts, vitamins, and amino acids. A key difference in IMDM is the greater
478 abundance of aromatic amino acids that are precursors of endogenous agonists for the
479 arylhydrocarbon receptor (AhR) that drives Th17 differentiation (39). It is possible that
480 AhR activity alters gene expression in ways that reprogram T cells to be less dependent
481 on S6K2. In support, addition of an exogenous AhR ligand FICZ corrected the Th17
482 differentiation defect in S6K2$^{-/-}$ T cells.

483 We chose to assess Th17 differentiation *in vivo* using the MOG_{35-55}-induced model of
484 EAE, since chemical and genetic approaches have established a role for mTORC1 in this

model (13, 14, 19, 20). As expected, rapamycin treatment muted clinically apparent EAE symptoms and reduced the percentage of IL-17A^{+} as well as IFNγ^{+} cells in the spinal cord. However, S6K2$^{-/-}$ mice showed no difference in clinical scores or inflammatory T cells. This result suggests that selective targeting of S6K2 has limited potential for the treatment of T cell-mediated autoimmunity. Another implication of this result is that *in vitro* Th17 differentiation in IMDM, compared to RPMI, provided a better prediction of *in vivo* outcomes. Differences in media composition might underlie some of the differences reported among various studies of specific mTORC1 pathway components in T helper differentiation (9, 13, 14).

mTOR inhibition enhances the formation of induced Tregs (13, 15), yet the relevant downstream substrates involved in this effect are not clear. Interestingly, naïve S6K2$^{-/-}$ T cells had an increased propensity to differentiate into FoxP3^{+} cells under Treg biasing conditions *in vitro*, regardless of the media used. The increase was consistent across experiments but quantitatively modest, with the percent FoxP3^{+} cells averaging 26% for WT and 35% for S6K2$^{-/-}$ T cells. In addition, the significant increase seen in Treg generation in 10 days MOG immunized S6K2$^{-/-}$ mice suggests a milder inflammatory model may benefit from inhibition of S6K2. Further studies are needed to determine whether this increase in induced Treg generation influences the severity of other autoimmune disease models and anti-tumor immunity. Notably, S6K2$^{-/-}$ mice had normal numbers of nTregs with similar suppressive potential as WT nTregs.

Both S6K1 and S6K2 are expressed in T cells and contribute to robust phosphorylation of S6 and other substrates following TCR stimulation. However, it remains unclear how these kinases contribute to T cell activation and function. Though

Sasaki and colleagues have shown S6K1 knockout mice to have decreased Th17 differentiation *in vitro*, their EAE studies showed no improvement in clinical scores (38). Taken in consideration with our own *in vivo* studies suggest S6Ks to not be a main mTORC1 downstream effector in driving EAE pathogenesis. Therefore, the efficacy of rapamycin in the EAE model might be the result of blocking T cell clonal expansion and/or a specific effect on T helper differentiation. We initiated treatment several days after immunization to minimize effects on proliferation. This suggests that rapamycin targets other mTORC1 downstream substrates to produce significantly delayed and improved clinical scores in EAE. It is possible that S6Ks have a more prominent function in other autoimmune conditions or in certain T cell responses to infection.

There is interest in targeting S6K2 for cancer treatment, as over 88% of tumors express higher levels than corresponding healthy tissues (52–56). Selective chemical inhibitors of S6K2 have not yet been described. Should such compounds become available, the data presented here suggest that blockade of S6K2 will not be broadly immunosuppressive compared to rapamycin. Selective inhibition or conditional deletion of S6K1 and S6K2 in various cell types will be necessary to achieve a more detailed understanding of the unique and shared functions of these kinases in different aspects of the immune response.

Acknowledgments

The authors thank Yumay Chen and Ping H. Wang (UC Irvine) for use and assistance of the Seahorse XF24 analyzer, and Lindsey Araujo, Adam K. Idica, and Sara E. Lutz for technical advice. We are grateful to Sara Kozma (IDIBELL) for providing the S6K2$^{-/-}$ mouse strain, originally generated at the Friedrich Miescher Institute.

References

1. Laplante, M., and D. M. Sabatini. 2012. mTOR signaling in growth control and disease. *Cell* 149: 274–293.

2. Cybulski, N., and M. N. Hall. 2009. TOR complex 2: a signaling pathway of its own. *Trends Biochem Sci* 34: 620–627.

3. Finlay, D., and D. A. Cantrell. 2011. Metabolism, migration and memory in cytotoxic T cells. *Nat Rev Immunol* 11: 109–117.

4. Okkenhaug, K. 2013. Signaling by the phosphoinositide 3-kinase family in immune cells. *Annu Rev Immunol* 31: 675–704.

5. Zeng, H., and H. Chi. 2013. mTOR and lymphocyte metabolism. *Curr Opin Immunol* 25: 347–355.

6. Powell, J. D., K. N. Pollizzi, E. B. Heikamp, and M. R. Horton. 2012. Regulation of immune responses by mTOR. *Annu Rev Immunol* 30: 39–68.

7. Magnuson, B., B. Ekim, and D. C. Fingar. 2012. Regulation and function of ribosomal protein S6 kinase (S6K) within mTOR signalling networks. *Biochem J* 441: 1–21.

8. Lawrence, J. C., and R. T. Abraham. 1997. PHAS/4E-BPs as regulators of mRNA translation and cell proliferation. *Trends Biochem Sci* 22: 345–349.

9. Yang, K., S. Shrestha, H. Zeng, P. W. Karmaus, G. Neale, P. Vogel, D. A. Guertin, R. F. Lamb, and H. Chi. 2013. T cell exit from quiescence and differentiation into Th2 cells depend on Raptor-mTORC1-mediated metabolic reprogramming. *Immunity* 39: 1043–1056.

10. Michalek, R. D., V. A. Gerriets, S. R. Jacobs, A. N. Macintyre, N. J. MacIver, E. F. Mason, S. A. Sullivan, A. G. Nichols, and J. C. Rathmell. 2011. Cutting edge: distinct

560 glycolytic and lipid oxidative metabolic programs are essential for effector and
561 regulatory CD4+ T cell subsets. *J Immunol* 186: 3299–3303.
562 11. Shi, L. Z., R. Wang, G. Huang, P. Vogel, G. Neale, D. R. Green, and H. Chi. 2011.
563 HIF1alpha-dependent glycolytic pathway orchestrates a metabolic checkpoint for the
564 differentiation of TH17 and Treg cells. *J Exp Med* 208: 1367–1376.
565 12. Zeng, H., K. Yang, C. Cloer, G. Neale, P. Vogel, and H. Chi. 2013. mTORC1 couples
566 immune signals and metabolic programming to establish T(reg)-cell function. *Nature*
567 499: 485–490.
568 13. Delgoffe, G. M., K. N. Pollizzi, A. T. Waickman, E. Heikamp, D. J. Meyers, M. R.
569 Horton, B. Xiao, P. F. Worley, and J. D. Powell. 2011. The kinase mTOR regulates
570 the differentiation of helper T cells through the selective activation of signaling by
571 mTORC1 and mTORC2. *Nat Immunol* 12: 295–303.
572 14. Kurebayashi, Y., S. Nagai, A. Ikejiri, M. Ohtani, K. Ichiyama, Y. Baba, T. Yamada,
573 S. Egami, T. Hoshii, A. Hirao, S. Matsuda, and S. Koyasu. 2012. PI3K-Akt-
574 mTORC1-S6K1/2 axis controls Th17 differentiation by regulating Gfi1 expression
575 and nuclear translocation of RORγ. *Cell Rep* 1: 360–373.
576 15. Delgoffe, G. M., T. P. Kole, Y. Zheng, P. E. Zarek, K. L. Matthews, B. Xiao, P. F.
577 Worley, S. C. Kozma, and J. D. Powell. 2009. The mTOR kinase differentially
578 regulates effector and regulatory T cell lineage commitment. *Immunity* 30: 832–844.
579 16. Procaccini, C., V. De Rosa, M. Galgani, L. Abanni, G. Calì, A. Porcellini, F.
580 Carbone, S. Fontana, T. L. Horvath, A. La Cava, and G. Matarese. 2010. An
581 oscillatory switch in mTOR kinase activity sets regulatory T cell responsiveness.
582 *Immunity* 33: 929–941.

583 17. Park, Y., H. S. Jin, J. Lopez, C. Elly, G. Kim, M. Murai, M. Kronenberg, and Y. C.
584 Liu. 2013. TSC1 regulates the balance between effector and regulatory T cells. *J Clin*
585 *Invest* 123: 5165–5178.
586 18. Branisteanu, D. D., C. Mathieu, and R. Bouillon. 1997. Synergism between sirolimus
587 and 1,25-dihydroxyvitamin D3 in vitro and in vivo. *J Neuroimmunol* 79: 138–147.
588 19. Esposito, M., F. Ruffini, M. Bellone, N. Gagliani, M. Battaglia, G. Martino, and R.
589 Furlan. 2010. Rapamycin inhibits relapsing experimental autoimmune
590 encephalomyelitis by both effector and regulatory T cells modulation. *J*
591 *Neuroimmunol* 220: 52–63.
592 20. Donia, M., K. Mangano, A. Amoroso, M. C. Mazzarino, R. Imbesi, P.
593 Castrogiovanni, M. Coco, P. Meroni, and F. Nicoletti. 2009. Treatment with
594 rapamycin ameliorates clinical and histological signs of protracted relapsing
595 experimental allergic encephalomyelitis in Dark Agouti rats and induces expansion of
596 peripheral CD4+CD25+Foxp3+ regulatory T cells. *J Autoimmun* 33: 135–140.
597 21. Lisi, L., P. Navarra, R. Cirocchi, A. Sharp, E. Stigliano, D. L. Feinstein, and C. Dello
598 Russo. 2012. Rapamycin reduces clinical signs and neuropathic pain in a chronic
599 model of experimental autoimmune encephalomyelitis. *J Neuroimmunol* 243: 43–51.
600 22. Carlson, R. P., W. L. Baeder, R. G. Caccese, L. M. Warner, and S. N. Sehgal. 1993.
601 Effects of orally administered rapamycin in animal models of arthritis and other
602 autoimmune diseases. *Ann N Y Acad Sci* 685: 86–113.
603 23. Harrison, D. E., R. Strong, Z. D. Sharp, J. F. Nelson, C. M. Astle, K. Flurkey, N. L.
604 Nadon, J. E. Wilkinson, K. Frenkel, C. S. Carter, M. Pahor, M. A. Javors, E.

605 Fernandez, and R. A. Miller. 2009. Rapamycin fed late in life extends lifespan in
606 genetically heterogeneous mice. *Nature* 460: 392–395.
607 24. Perl, A. 2015. mTOR activation is a biomarker and a central pathway to autoimmune
608 disorders, cancer, obesity, and aging. *Ann N Y Acad Sci* 1346: 33–44.
609 25. Perl, A. 2016. Activation of mTOR (mechanistic target of rapamycin) in rheumatic
610 diseases. *Nat Rev Rheumatol* 12: 169–182.
611 26. Lai, Z. W., R. Borsuk, A. Shadakshari, J. Yu, M. Dawood, R. Garcia, L. Francis, H.
612 Tily, A. Bartos, S. V. Faraone, P. Phillips, and A. Perl. 2013. Mechanistic target of
613 rapamycin activation triggers IL-4 production and necrotic death of double-negative
614 T cells in patients with systemic lupus erythematosus. *J Immunol* 191: 2236–2246.
615 27. Fischer, K. E., J. A. Gelfond, V. Y. Soto, C. Han, S. Someya, A. Richardson, and S.
616 N. Austad. 2015. Health Effects of Long-Term Rapamycin Treatment: The Impact on
617 Mouse Health of Enteric Rapamycin Treatment from Four Months of Age throughout
618 Life. *PLoS ONE* 10: e0126644.
619 28. Pallet, N., and C. Legendre. 2013. Adverse events associated with mTOR inhibitors.
620 *Expert Opin Drug Saf* 12: 177–186.
621 29. Nardella, C., A. Lunardi, G. Fedele, J. G. Clohessy, A. Alimonti, S. C. Kozma, G.
622 Thomas, M. Loda, and P. P. Pandolfi. 2011. Differential expression of S6K2 dictates
623 tissue-specific requirement for S6K1 in mediating aberrant mTORC1 signaling and
624 tumorigenesis. *Cancer Res* 71: 3669–3675.
625 30. Shima, H., M. Pende, Y. Chen, S. Fumagalli, G. Thomas, and S. C. Kozma. 1998.
626 Disruption of the p70(s6k)/p85(s6k) gene reveals a small mouse phenotype and a new
627 functional S6 kinase. *EMBO J* 17: 6649–6659.

628 31. Pelletier, J., J. Graff, D. Ruggero, and N. Sonenberg. 2015. Targeting the eIF4F
629 translation initiation complex: a critical nexus for cancer development. *Cancer Res*
630 75: 250–263.
631 32. Chung, J., C. J. Kuo, G. R. Crabtree, and J. Blenis. 1992. Rapamycin-FKBP
632 specifically blocks growth-dependent activation of and signaling by the 70 kd S6
633 protein kinases. *Cell* 69: 1227–1236.
634 33. Kuo, C. J., J. Chung, D. F. Fiorentino, W. M. Flanagan, J. Blenis, and G. R. Crabtree.
635 1992. Rapamycin selectively inhibits interleukin-2 activation of p70 S6 kinase.
636 *Nature* 358: 70–73.
637 34. Choo, A. Y., S. O. Yoon, S. G. Kim, P. P. Roux, and J. Blenis. 2008. Rapamycin
638 differentially inhibits S6Ks and 4E-BP1 to mediate cell-type-specific repression of
639 mRNA translation. *Proc Natl Acad Sci U S A* 105: 17414–17419.
640 35. Salmond, R. J., R. J. Brownlie, O. Meyuhas, and R. Zamoyska. 2015. Mechanistic
641 Target of Rapamycin Complex 1/S6 Kinase 1 Signals Influence T Cell Activation
642 Independently of Ribosomal Protein S6 Phosphorylation. *J Immunol* 195: 4615–4622.
643 36. So, L., J. Lee, M. Palafox, S. Mallya, C. Woxland, M. Arguello, M. Truitt, N.
644 Sonenberg, D. Ruggero, and D. A. Fruman. 2016. The 4E-BP/eIF4E axis controls
645 rapamycin-sensitive growth and proliferation in lymphocytes. *submitted* .
646 37. Pende, M., S. H. Um, V. Mieulet, M. Sticker, V. L. Goss, J. Mestan, M. Mueller, S.
647 Fumagalli, S. C. Kozma, and G. Thomas. 2004. S6K1(-/-)/S6K2(-/-) mice exhibit
648 perinatal lethality and rapamycin-sensitive 5'-terminal oligopyrimidine mRNA
649 translation and reveal a mitogen-activated protein kinase-dependent S6 kinase
650 pathway. *Mol Cell Biol* 24: 3112–3124.

651 38. Sasaki, C. Y., G. Chen, R. Munk, E. Eitan, J. Martindale, D. L. Longo, and P. Ghosh.
652 2016. p(70S6K1) in the TORC1 pathway is essential for the differentiation of Th17
653 Cells, but not Th1, Th2, or Treg cells in mice. *Eur J Immunol* 46: 212–222.
654 39. Veldhoen, M., K. Hirota, J. Christensen, A. O'Garra, and B. Stockinger. 2009.
655 Natural agonists for aryl hydrocarbon receptor in culture medium are essential for
656 optimal differentiation of Th17 T cells. *J Exp Med* 206: 43–49.
657 40. Perez, O. D., and G. P. Nolan. 2006. Phospho-proteomic immune analysis by flow
658 cytometry: from mechanism to translational medicine at the single-cell level.
659 *Immunol Rev* 210: 208–228.
660 41. Tolcher, A., J. Goldman, A. Patnaik, K. P. Papadopoulos, P. Westwood, C. S. Kelly,
661 W. Bumgardner, L. Sams, S. Geeganage, T. Wang, A. R. Capen, J. Huang, S. Joseph,
662 J. Miller, K. A. Benhadji, L. H. Brail, and L. S. Rosen. 2014. A phase I trial of
663 LY2584702 tosylate, a p70 S6 kinase inhibitor, in patients with advanced solid
664 tumours. *Eur J Cancer* 50: 867–875.
665 42. Wan, X., B. Harkavy, N. Shen, P. Grohar, and L. J. Helman. 2007. Rapamycin
666 induces feedback activation of Akt signaling through an IGF-1R-dependent
667 mechanism. *Oncogene* 26: 1932–1940.
668 43. Sridharan, S., and A. Basu. 2011. S6 kinase 2 promotes breast cancer cell survival via
669 Akt. *Cancer Res* 71: 2590–2599.
670 44. Robitaille, A. M., S. Christen, M. Shimobayashi, M. Cornu, L. L. Fava, S. Moes, C.
671 Prescianotto-Baschong, U. Sauer, P. Jenoe, and M. N. Hall. 2013. Quantitative
672 phosphoproteomics reveal mTORC1 activates de novo pyrimidine synthesis. *Science*
673 339: 1320–1323.

45. Ben-Sahra, I., J. J. Howell, J. M. Asara, and B. D. Manning. 2013. Stimulation of de novo pyrimidine synthesis by growth signaling through mTOR and S6K1. *Science* 339: 1323–1328.

46. Langrish, C. L., Y. Chen, W. M. Blumenschein, J. Mattson, B. Basham, J. D. Sedgwick, T. McClanahan, R. A. Kastelein, and D. J. Cua. 2005. IL-23 drives a pathogenic T cell population that induces autoimmune inflammation. *J Exp Med* 201: 233–240.

47. Park, H., Z. Li, X. O. Yang, S. H. Chang, R. Nurieva, Y. H. Wang, Y. Wang, L. Hood, Z. Zhu, Q. Tian, and C. Dong. 2005. A distinct lineage of CD4 T cells regulates tissue inflammation by producing interleukin 17. *Nat Immunol* 6: 1133–1141.

48. Eisenstein, E. M., and C. B. Williams. 2009. The T(reg)/Th17 cell balance: a new paradigm for autoimmunity. *Pediatr Res* 65: 26R–31R.

49. Pollizzi, K. N., A. T. Waickman, C. H. Patel, I. H. Sun, and J. D. Powell. 2015. Cellular size as a means of tracking mTOR activity and cell fate of CD4+ T cells upon antigen recognition. *PLoS ONE* 10: e0121710.

50. Hsu, P. P., S. A. Kang, J. Rameseder, Y. Zhang, K. A. Ottina, D. Lim, T. R. Peterson, Y. Choi, N. S. Gray, M. B. Yaffe, J. A. Marto, and D. M. Sabatini. 2011. The mTOR-regulated phosphoproteome reveals a mechanism of mTORC1-mediated inhibition of growth factor signaling. *Science* 332: 1317–1322.

51. Yu, Y., S. O. Yoon, G. Poulogiannis, Q. Yang, X. M. Ma, J. Villén, N. Kubica, G. R. Hoffman, L. C. Cantley, S. P. Gygi, and J. Blenis. 2011. Phosphoproteomic analysis

identifies Grb10 as an mTORC1 substrate that negatively regulates insulin signaling. *Science* 332: 1322–1326.

52. Pérez-Tenorio, G., E. Karlsson, M. A. Waltersson, B. Olsson, B. Holmlund, B. Nordenskjöld, T. Fornander, L. Skoog, and O. Stål. 2011. Clinical potential of the mTOR targets S6K1 and S6K2 in breast cancer. *Breast Cancer Res Treat* 128: 713–723.

53. Filonenko, V. V., R. Tytarenko, S. K. Azatjan, L. O. Savinska, Y. A. Gaydar, I. T. Gout, V. S. Usenko, and V. V. Lyzogubov. 2004. Immunohistochemical analysis of S6K1 and S6K2 localization in human breast tumors. *Exp Oncol* 26: 294–299.

54. Lyzogubov, V. V., D. I. Lytvyn, T. M. Dudchenko, N. V. Lubchenko, P. V. Pogrybniy, S. V. Nespryadko, A. B. Vinnitska, V. S. Usenko, I. T. Gout, and V. V. Filonenko. 2004. Immunohistochemical analysis of S6K1 and S6K2 expression in endometrial adenocarcinomas. *Exp Oncol* 26: 287–293.

55. Pardo, O. E., C. Wellbrock, U. K. Khanzada, M. Aubert, I. Arozarena, S. Davidson, F. Bowen, P. J. Parker, V. V. Filonenko, I. T. Gout, N. Sebire, R. Marais, J. Downward, and M. J. Seckl. 2006. FGF-2 protects small cell lung cancer cells from apoptosis through a complex involving PKCepsilon, B-Raf and S6K2. *EMBO J* 25: 3078–3088.

56. Pardo, O. E., and M. J. Seckl. 2013. S6K2: The Neglected S6 Kinase Family Member. *Front Oncol* 3: 191.

Figure legends

Figure 1: *S6K2*$^{-/-}$ mice have normal T cell compartments and CD4^{+} T cells display normal activation marker upregulation. **(A)** Flow cytometry analysis of CD4^{+} and CD8^{+} populations in the thymus, spleen, and lymph nodes from a representative experiment in (B). **(B)** Quantitative analysis of CD4^{+}, CD8^{+}, and CD4^{+}CD8^{+} populations in the thymus, spleen, and lymph nodes (numbers indicate millions, mean +/- SEM, n = 3 independent experiments). **(C)** nTreg populations were analyzed by CD4^{+}CD25^{+} expression in the thymus, spleen, and lymph nodes. Average percentage mean (from total CD4^{+} populations) +/- SEM is shown below (n = 3 independent experiments). **(D)** Flow cytometry analysis of activation markers and cell size (forward scatter; FSC) of WT and *S6K2*$^{-/-}$ T cells after 24 hr of stimulation using varying concentrations of anti-CD3 under neutral conditions (n = 3 independent experiments).

Figure 2: *S6K2*$^{-/-}$ CD4 T cells have reduced S6 phosphorylation during the first 24 hours of stimulation compared to WT, but have comparable proliferation and cell size under neutral stimulation conditions. **(A)** Histogram overlays of p-S6 comparing WT and *S6K2*$^{-/-}$ CD4 T cells during a time course of neutral stimulation, representative of 3 independent experiments. **(B)** *Left,* Graph of normalized average mean fluorescence intensities (MFIs) of p-S6 in 24hr-activated CD4 T cells, * $p < 0.05$ (n = 5 independent experiments). Error bars indicate SEM. *Right*, The percentage of p-S6-positive T cells was graphed for 6 independent experiments comparing WT and *S6K2*$^{-/-}$ CD4 T cells after 24hr stimulation. The Wilcoxon signed-rank test was used to assess p value. **(C)** CFSE and p-S6 staining of WT and *S6K2*$^{-/-}$ naïve CD4^{+} T cells unstimulated or stimulated for 3

days, representative of 3 independent experiments. **(D)** CFSE histogram overlay of WT and *S6K2*$^{-/-}$ T cells from (C). **(E)** Cell size histogram overlay WT and *S6K2*$^{-/-}$ naïve CD4^{+} T cells stimulated for 24 hours. **(F)** Average FSC MFI plotted from (E) is shown, * p < 0.05 (n = 3 independent experiements). Error bars indicate SEM.

Figure 3: S6K2 and S6K1 have distinct substrates in activated T cells and have different roles in feedback to Akt. **(A)** Immunoblot analysis of lysates from WT and *S6K2*$^{-/-}$ naïve CD4^{+} T cells unstimulated or stimulated for 24 hours, representative of 3 independent experiments. Rapamycin (+rap) or S6K1 inhibitor (S6Ki) was included during stimulation in the samples indicated. Antibodies used to probe the blots are shown on the left. **(B)** Analysis of phospho CAD and S6K1 expression from immunoblots, mean +/- SEM, n = 3 independent experiments. *p < 0.05. **(C)** Intracellular phosphoflow staining of Akt and analysis by normalized MFI, mean +/- SEM, n = 3 independent experiments. *p < 0.05.

Figure 4: Naïve *S6K2*$^{-/-}$ CD4^{+} T cells generate fewer Treg and more Th17 cells, with little effect on Th1, Th17, or Treg proliferation. **(A)** Intracellular staining of IL-17A, FoxP3, and IFNγ in WT and *S6K2*$^{-/-}$ T cells stained with CFSE for cell division tracking. Naïve WT or *S6K2*$^{-/-}$ CD4^{+} T cells were cultured in RPMI media under indicated conditions for 4 days. Shown plots are representative of data analyzed in (B). **(B)** Paired analysis of IL-17A and IFNγ positive cells from multiple experiments performed as in (A) (Th17: n = 4 independent experiments, Treg: n = 5 independent experiments). The Wilcoxon signed-rank test was used to assess p value. **(C)** Histogram overlays of CFSE-

764 labeled T cells from (A). **(D)** IL-17 and IL-10 cytokine measurements by ELISA from the
765 supernatant of WT and *S6K2*$^{-/-}$ T cells cultured in Th17 or Treg skewing conditions for 4
766 days (mean +/- SEM, n = 3 independent experiments).
767
768 **Figure 5:** *S6K2*$^{-/-}$ and WT mice exhibit comparable EAE development. **(A)** Clinical
769 scores of EAE-induced WT and *S6K2*$^{-/-}$ mice (mean +/- SEM, n = 8 for each group). **(B)**
770 Clinical scores of EAE-induced WT, WT treated with Rap or vehicle (Veh), and *S6K2*$^{-/-}$
771 mice (mean +/- SEM, n = 3 for each group). **(C)** Graphed analysis of IFNγ and IL-17A
772 positive CD4^{+} T cells in the spinal cord of EAE-induced mice from (B), * $p < 0.05$ (mean
773 +/- SEM, n = 3). **(D)** pS6 (MFI and % positive) in CD4^{+} T cells from freshly harvested
774 lymph nodes from 10 day MOG immunized WT and *S6K2*$^{-/-}$ mice (mean +/- SEM, n = 3).
775 **(E)** CD4^{+}IL17A^{+} (% positive and MFI) and CD4^{+}FoxP3^{+} (% positive) populations in 3
776 day MOG restimulated splenocytes harvested from the same mice as used in (D) (mean
777 +/- SEM, n = 3).
778
779 **Figure 6:** IMDM rescues Th17 differentiation in S6K2$^{-/-}$ T cells. **(A)** Intracellular
780 staining of IL-17A and FoxP3 in WT and *S6K2*$^{-/-}$ T cells stained with CFSE. Naïve WT
781 or *S6K2*$^{-/-}$ CD4^{+} T cells were cultured under indicated conditions for 4 days in RPMI or
782 IMDM. Plots are representative of 3 independent experiments. **(B)** Comparative flow
783 cytometric analysis and quantitative analysis for normalized MFI of p-S6 signaling
784 between WT and *S6K2*$^{-/-}$ T cells 24 hr of neutral stimulation, *$p < 0.05$ (mean +/- SEM, n
785 = 3 independent experiments). **(C)** IL-17 and IL-10 cytokine measurements by ELISA
786 from the supernatant of WT and *S6K2*$^{-/-}$ T cells cultured in Th17 or Treg skewing

conditions for 4 days (mean +/- SEM, n = 3 independent experiments). **(D)** Intracellular staining of IL-17A in CFSE-labeled WT and *S6K2*$^{-/-}$ T cells cultured in Th17 skewing conditions for 4 days in RPMI, RPMI +FICZ, or IMDM. Plots are representative of 3 independent experiments.

Figure 1

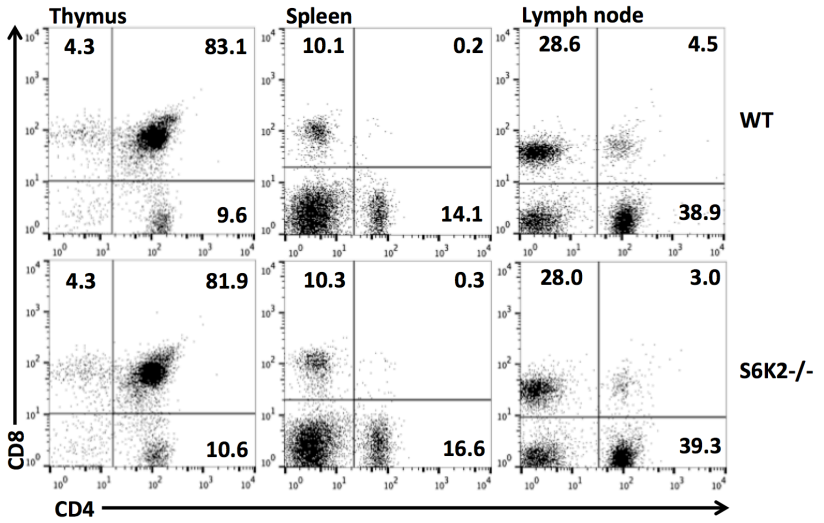

B

Thymus

	CD4+	CD8+	CD4+CD8+
WT	10.5± 1.6	5.6± 0.6	79.3± 2.6
S6K2-/-	11.6± .52	5.9± 1.2	76.7± 3.0

Spleen

	CD4+	CD8+	CD4-CD8-
WT	15.5±1.2	9.6± 1.3	74.8± 2.4
S6K2-/-	14.4± .37	9.4± 0.9	76.2± 1.2

Lymph Node

	CD4+	CD8+	CD4-CD8-
WT	33.8± 2.6	28.2± 0.8	38.0± 2.7
S6K2-/-	31± 4.2	28± .5	40.7± 3.9

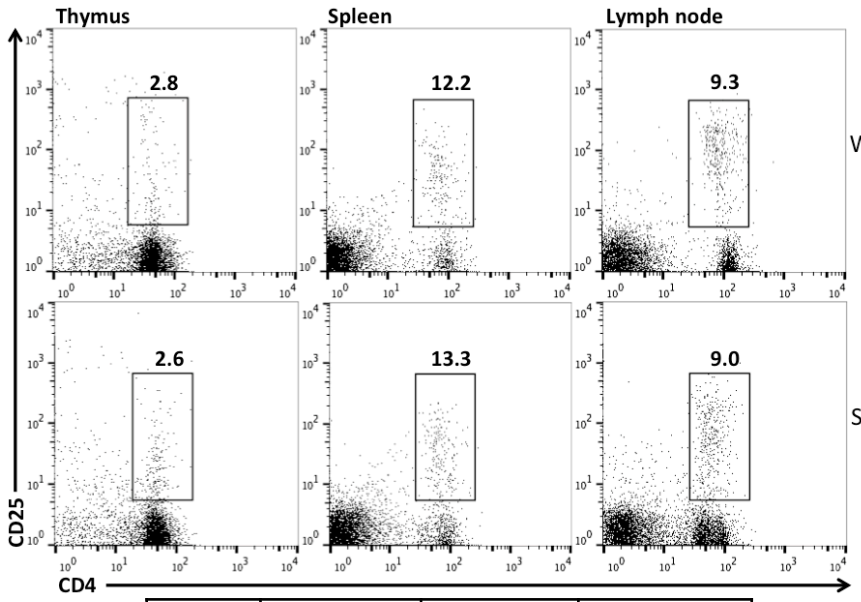

	Thymus	Spleen	Lymph Node
WT	2.5 ± .47	11.5 ± 1.3	10.1 ± .75
S6K2-/-	2.8 ± .46	11.3 ± 1.2	9.9 ± .1.9

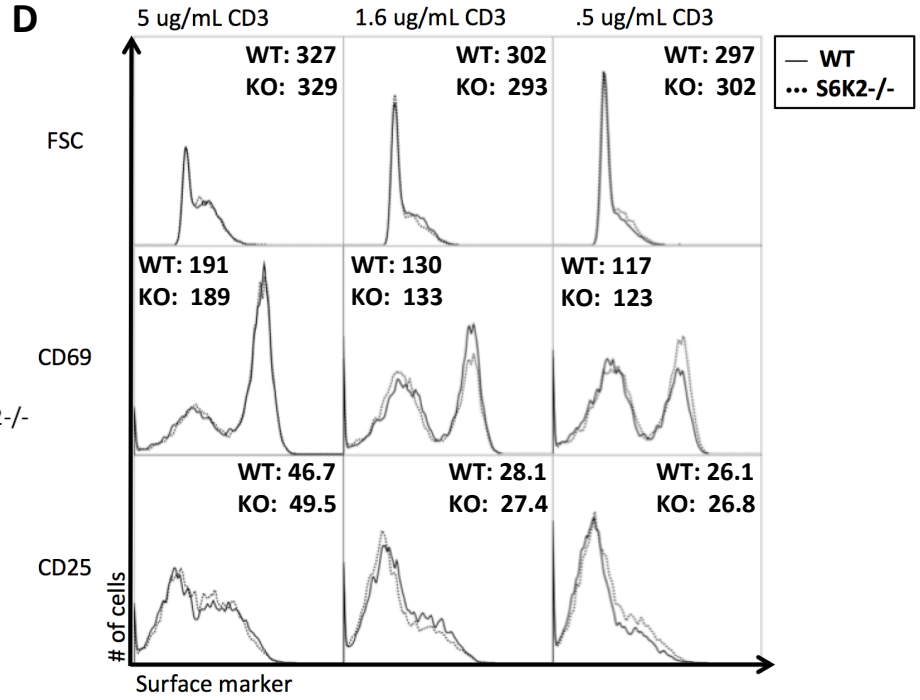

Figure 2

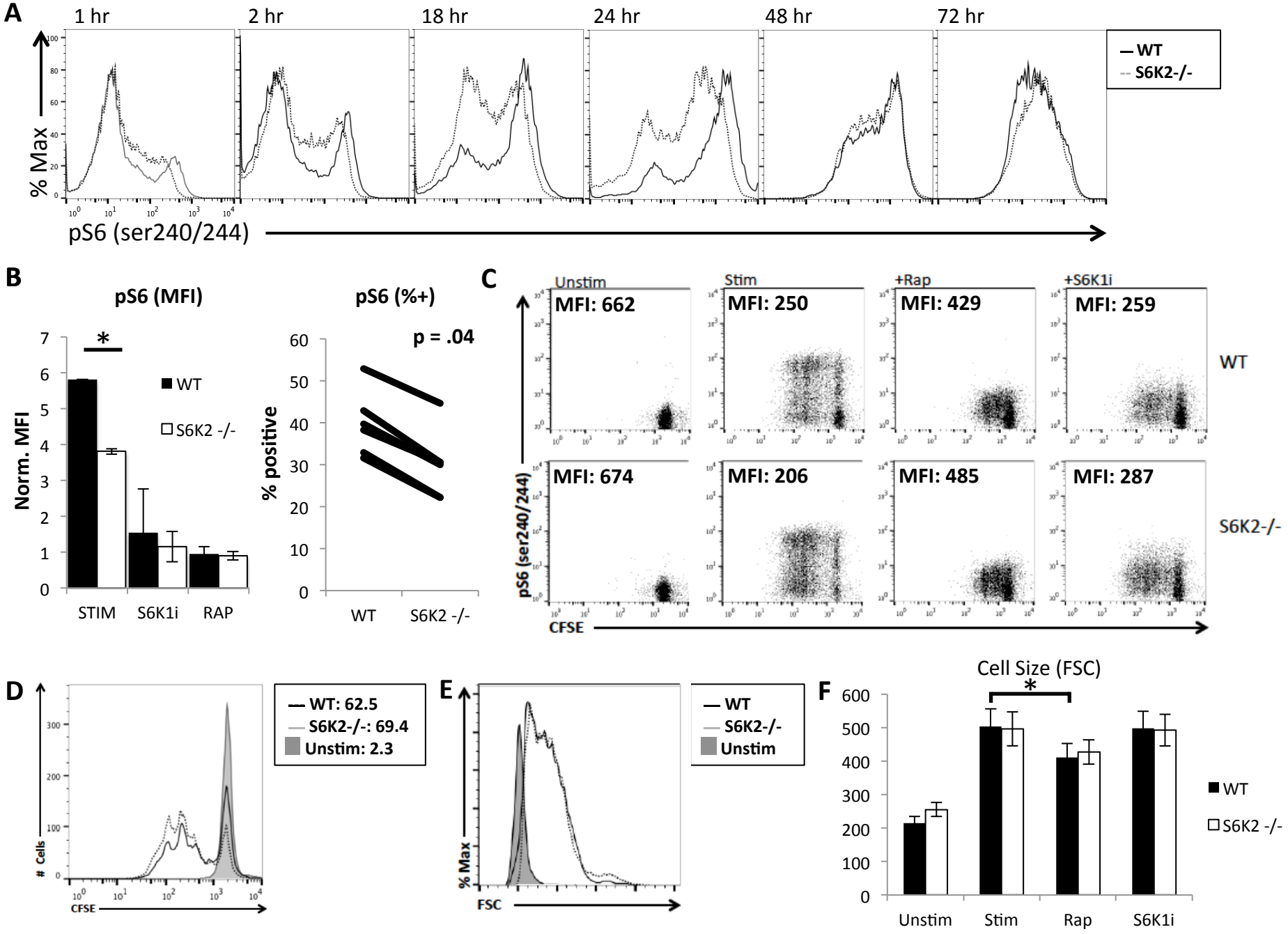
A
1 hr
2 hr
18 hr
24 hr
48 hr
72 hr
WT
S6K2-/-
% Max
pS6 (ser240/244)
B
pS6 (MFI)
pS6 (%+)
p = .04
Norm. MFI
% positive
WT
S6K2 -/-
STIM
S6K1i
RAP
C
Unstim
Stim
+Rap
+S6K1i
MFI: 662
MFI: 250
MFI: 429
MFI: 259
MFI: 674
MFI: 206
MFI: 485
MFI: 287
WT
S6K2-/-
pS6 (ser240/244)
CFSE
D
WT: 62.5
S6K2-/-: 69.4
Unstim: 2.3
Cells
CFSE
E
WT
S6K2-/-
Unstim
% Max
FSC
F
Cell Size (FSC)
WT
S6K2 -/-
Unstim
Stim
Rap
S6K1i

Figure 3

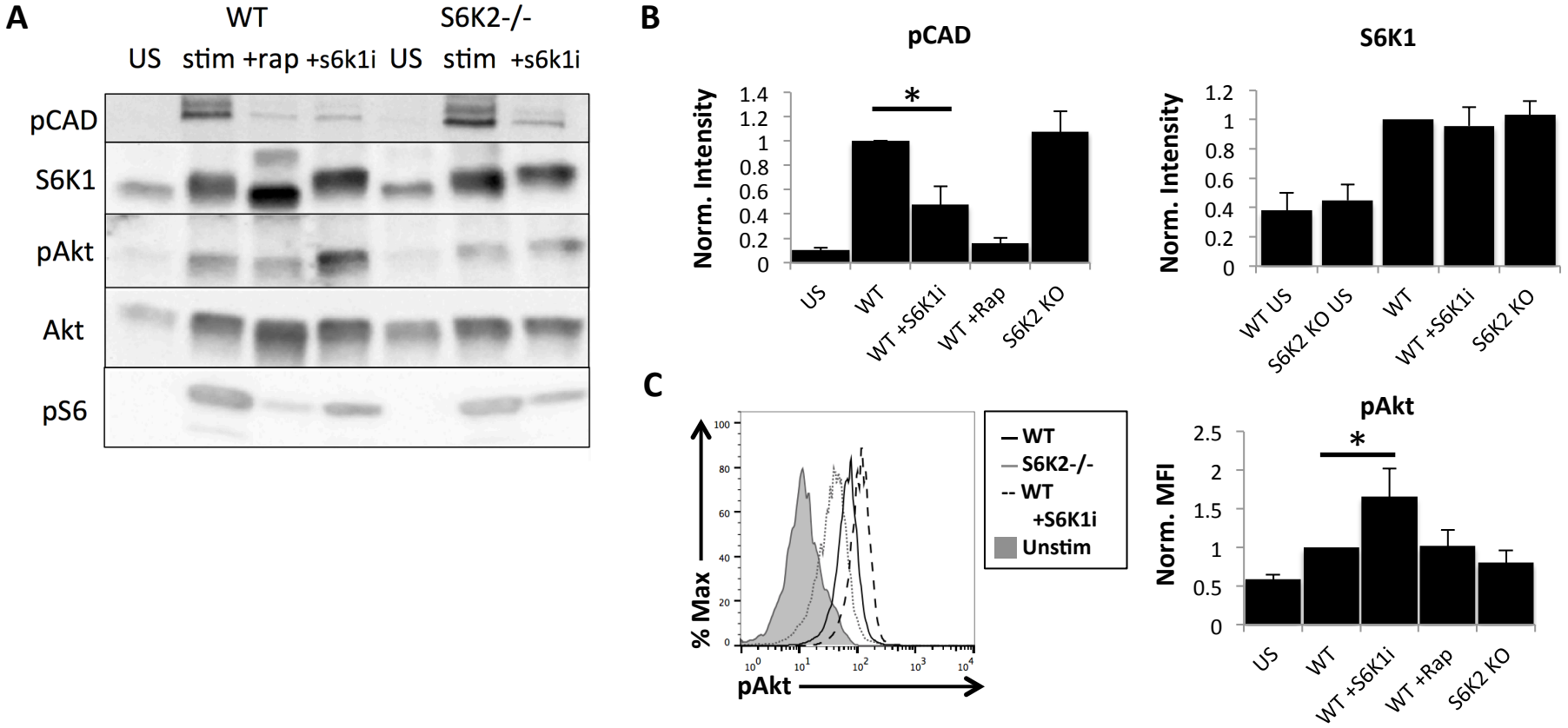
A
WT
S6K2-/-
US
stim
+rap
+s6k1i
US
stim
+s6k1i
pCAD
S6K1
pAkt
Akt
pS6
B
pCAD
Norm. Intensity
1.4
1.2
1
0.8
0.6
0.4
0.2
0
*
US
WT
WT +S6K1i
WT +Rap
S6K2 KO
S6K1
Norm. Intensity
1.2
1
0.8
0.6
0.4
0.2
0
WT US
S6K2 KO US
WT
WT +S6K1i
S6K2 KO
C
% Max
100
80
60
40
20
0
pAkt
WT
S6K2-/-
WT +S6K1i
Unstim
pAkt
Norm. MFI
2.5
2
1.5
1
0.5
0
*
US
WT
WT +S6K1i
WT +Rap
S6K2 KO

Figure 4

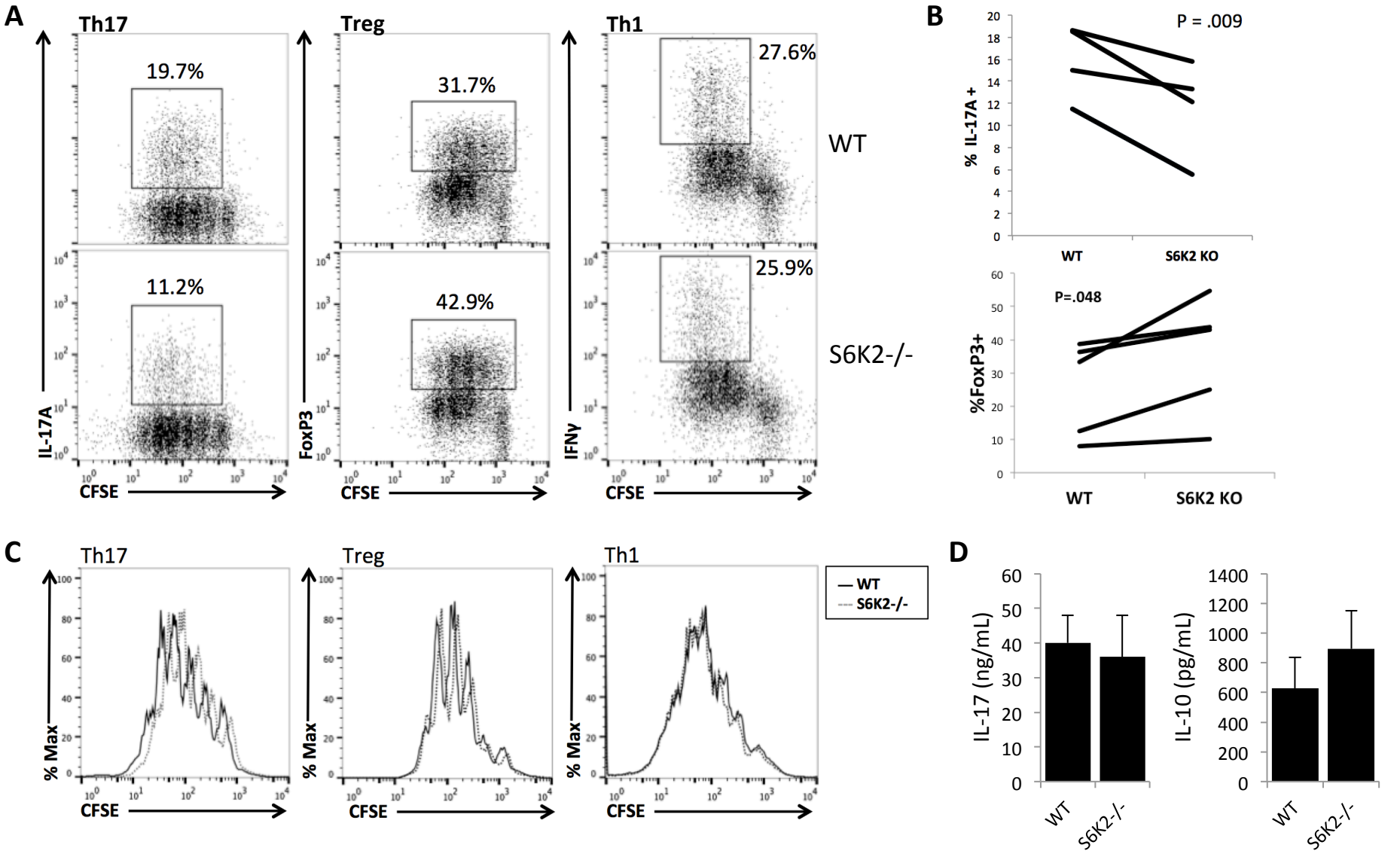
A
Th17
Treg
Th1
19.7%
31.7%
27.6%
11.2%
42.9%
25.9%
WT
S6K2-/-
IL-17A
FoxP3
IFNγ
CFSE
B
P = .009
% IL-17A +
WT
S6K2 KO
P=.048
%FoxP3+
C
Th17
Treg
Th1
WT
S6K2-/-
% Max
CFSE
D
IL-17 (ng/mL)
IL-10 (pg/mL)
WT
S6K2-/-

Figure 5

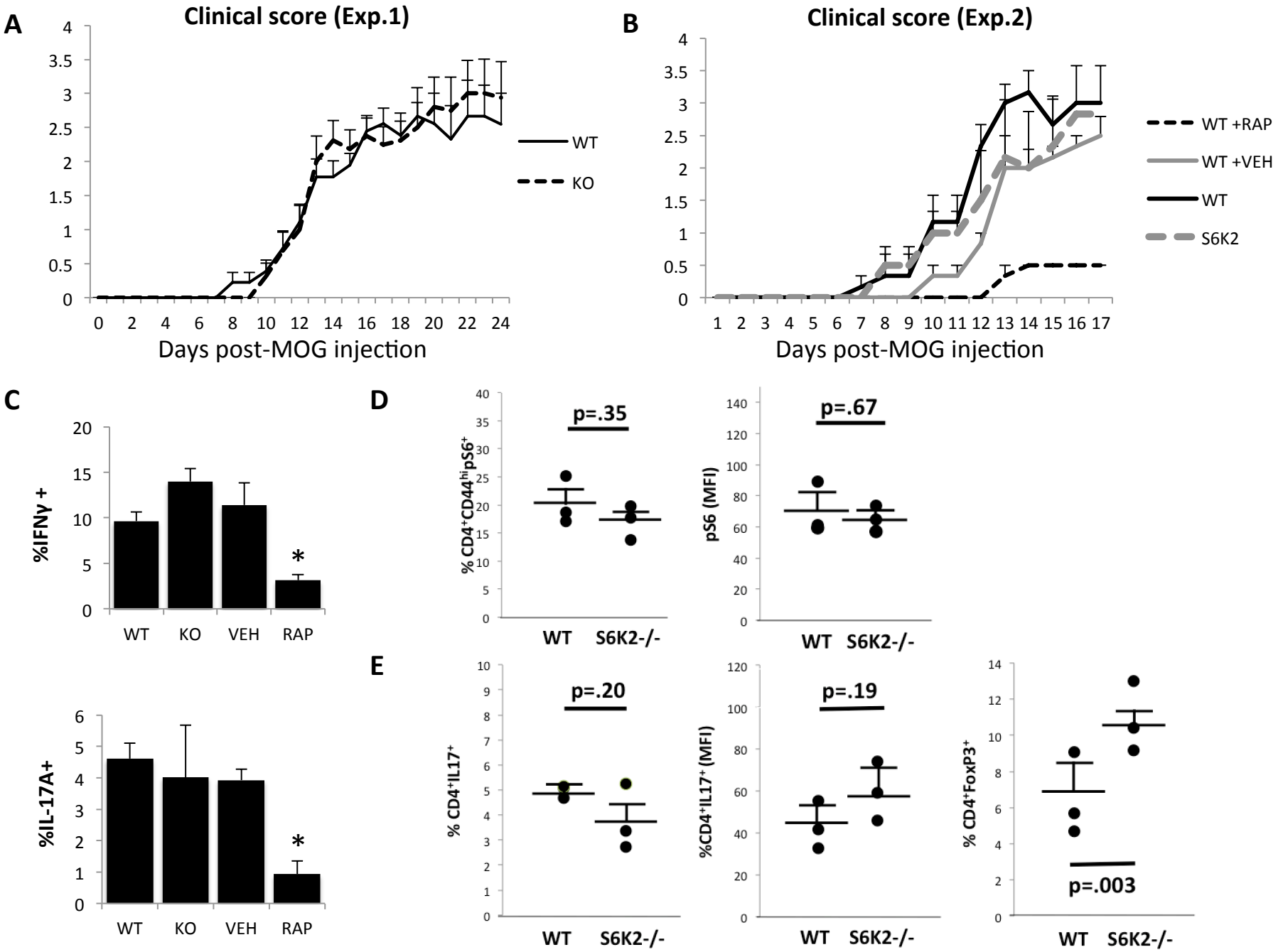
A
Clinical score (Exp.1)
Days post-MOG injection
WT
KO
B
Clinical score (Exp.2)
Days post-MOG injection
WT +RAP
WT +VEH
WT
S6K2
C
%IFNγ +
WT
KO
VEH
RAP
%IL-17A+
WT
KO
VEH
RAP
D
% CD4+CD44hipS6+
p=.35
WT
S6K2-/-
pS6 (MFI)
p=.67
WT
S6K2-/-
E
% CD4+IL17+
p=.20
WT
S6K2-/-
%CD4+IL17+ (MFI)
p=.19
WT
S6K2-/-
% CD4+FoxP3+
p=.003
WT
S6K2-/-

Figure 6

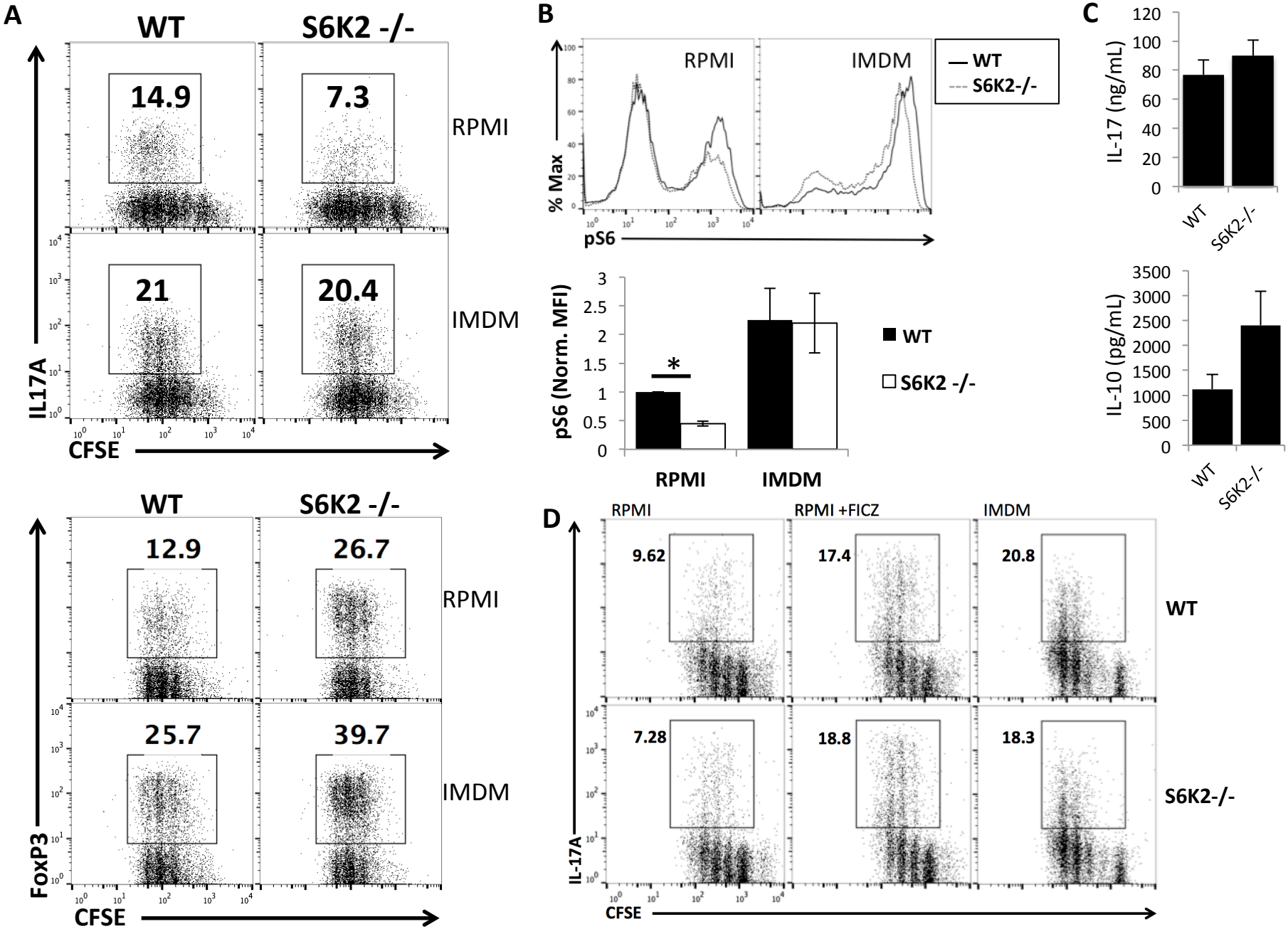
A
WT
S6K2 -/-
14.9
7.3
RPMI
21
20.4
IMDM
IL17A
CFSE
WT
S6K2 -/-
12.9
26.7
RPMI
25.7
39.7
IMDM
FoxP3
CFSE
B
RPMI
IMDM
WT
S6K2-/-
% Max
pS6
pS6 (Norm. MFI)
*
WT
S6K2 -/-
RPMI
IMDM
C
IL-17 (ng/mL)
WT
S6K2-/-
IL-10 (pg/mL)
WT
S6K2-/-
D
RPMI
RPMI +FICZ
IMDM
9.62
17.4
20.8
WT
7.28
18.8
18.3
S6K2-/-
IL-17A
CFSE